文章编号:1000-0887(2016)12-1378-16

Numerical Study on Coupling Effects of FPSO Ship Motion and LNG Tank Sloshing in Low-Filling Conditions*

ZHUANG Yuan, WAN De-cheng

(*State Key Laboratory of Ocean Engineering*(*Shanghai Jiao Tong University*);
School of Naval Architecture, Ocean & Civil Engineering, Shanghai Jiao Tong University;
Collaborative Innovation Center for Advanced Ship and Deep-Sea Exploration,
Shanghai 200240, *P.R.China*)

Abstract: In this paper, numerical simulations of FPSO ship motion coupled with LNG tank sloshing with low-filling ratios are conducted. The fully coupled problem is addressed with our own unsteady RANS solver: naoe-FOAM-SJTU developed based on the open source tool libraries of OpenFOAM. The internal tank sloshing and external wave flow are solved simultaneously. The FPSO model includes 2 LNG tanks. For the ship 3-DOFs are released in the regular beam waves. The filling ratios of the 2 tanks are 20% ~20% , lower than the external free surface. This kind of low-filling condition reduces ship roll motion significantly, and produces complex free surface shapes in tanks. 4 different incident wave frequencies are considered in the simulation in comparison with the existing experimental data. The comparison shows that the numerical results are in good agreement with the experimental data, proving the reliability of the proposed method. The filling conditions with large wave amplitudes are studied further, and due to the coupling effect, violent sloshing occurs in tanks and impulsive pressure forms on bulkhead.

Key words: LNG sloshing; coupled motion; low-filling condition; naoe-FOAM-SJTU solver
CLC number: O35 **Document code**: A
doi: 10.21656/1000-0887.370516

Introduction

The application of LNG and FPSO becomes popular in the last decades, thus the coupling effects of tank sloshing and ship motion are worth discussing. The ship motion excited by external waves influences the tank sloshing and the sloshing liquid in tanks affects the ship motion in return. The internal sloshing makes the prediction of ship motion different from those without tanks, and the violent sloshing in tanks excited by ship motion may cause large deformation and impulsive pressure on bulkhead, even damage the structure. When going through studies of ship motion coupled with partially filled tanks before, we found that in beam waves, low-filling tank conditions had some good effect on the anti-

* Received 2016-11-17; Revised 2016-12-09
Project supported by the National Natural Science Foundation of China (51379125; 51490675; 11432009; 51579145; 11272120) and the Chang Jiang Scholars Program of China(T2014099)
Corresponding author, WAN De-cheng, E-mail: dcwan@sjtu.edu.cn

rolling capability. However, the impulsive pressure on bulkhead in the low-filling condition is still obvious. Therefore, it is essential to study the ship motion coupled with low-filling sloshing tanks, which can give a prediction of ship motion and internal impulsive pressure accurately. On the one hand, the results of the study could provide a guide for ship and tank structural design; on the other hand, the sloshing in tanks may help enhance the stability against ship motion.

The studies on coupling effects of ship motion with tank sloshing can be traced back to early 1970's. Mikelis et al.[1] did some initial computations of coupled problems about sloshing and ship motion as well as experiments. Malenica et al.[2] studied the coupling effect using the linear potential theory, with the method of boundary integral equations implemented in both ship motion and tank sloshing. Kim[3] used the finite difference method (FDM) to simulate a 3D sloshing flow in tanks, where the finite element method (FEM) is applied to compute slosh-induced forces and moments. He chose a time-domain panel to compute the S175 hull ship motion. Kim et al.[4] applied the same method simulating the S175 hull. The tank filling ratios were mainly 30% and 60%. The anti-rolling phenomenon was observed in partially filled tanks. Nam et al.[5] conducted both numerical and experimental studies of the LNG FPSO model. They used the FEM to simulate the sloshing flows and computed ship motion with the impulsive-response function (IRF). 4 different filling ratios were considered for the roll motion response amplitude operators (RAOs).

The studies in recent decades has begun to use the viscous flow theory in order to solve the nonlinearity of the tank sloshing. In low-filling conditions, the flow in tanks become much more violent, thus the viscous flow theory becomes essential to simulate the complex free surface. The computational fluid dynamics (CFD) plays a vital role in numerical simulation, especially in solving the nonlinear surface and turbulent flow. Therefore, it is an effective way to simulate the coupling effect with the CFD method. Servún-Camas et al.[6] coupled a smooth particle hydrodynamics (SPH) solver for simulating internal flows in tanks with a finite element method solver for seakeeping problems. Since 2010, an open source tool packages, OpenFOAM, has become a popular way to do the numerical simulation. Li et al.[7] and Jiang et al.[8] both applied the viscous flow theory under OpenFOAM to compute violent flow in tanks. Jiang et al.[8] simulated the low-filling condition (20% ~ 20%) and observed the breaking surface in tanks and impulsive pressure on bulkhead. Sen[9] solved the internal flow based on OpenFOAM and the external ship motion with the 3D time domain transient Green's function.

However, the studies using OpenFOAM or other viscous flow theories all solved ship motion based on the potential theory, which ignores the influence of viscosity in the external region and the full coupling of ship motion and tank sloshing. Shen et al.[10] integrated a 6-DOF ship motion and wave generation module into OpenFOAM to form the in-house unsteady RANS solver: naoe-FOAM-SJTU. Wang et al.[11] simulated the sloshing performance

of 3D LNG tanks with the volume of fluid (VOF) method based on this solver. Shen et al.[12] realized the fully coupled methods for ship motion and tank sloshing through naoe-FOAM-SJTU. The simulation was done by solving the Navier-Stokes equation in both external and internal regions. A KVLCC2 model was chosen to compare the simulation with experimental results and then the coupling effects were observed in the KVLCC2 model with 2 LNG tanks.

In this paper, the coupling effects of ship motion in waves and LNG tank sloshing of low-filling ratios are discussed. The internal sloshing tank and external sea waves are treated as an entire computational domain. The viscosities in both internal and external fields are considered to achieve the fully coupled simulation. To validate the present CFD method, a LNG FPSO ship with 2 tanks is chosen as the model ship. The filling ratio is chosen to be 20% ~ 20%. The simulation results are compared with the experiments by Nam et al.[5] The coupling effects are observed in beam waves, especially in roll motion. The low-filling conditions is studied further with large wave amplitudes and different wave frequencies. The impact pressures on bulkhead are involved in the end.

1 Methodology

As we solved the ship motion and tank sloshing as a whole, the solution of the fluid fields is the same both in internal and external regions. Therefore, 2 main solutions to be considered are the ship motion and the nonlinear surface in tank sloshing. The former used 6-DOF module and the latter applied turbulence model. Both the external wave flow and the ship motion are solved with the methods described below.

1.1 Governing equations

The incompressible Reynolds-averaged Navier-Stokes equations are adopted to investigate the viscous flow. With the dynamic deformation mesh, the governing equations are

$$\nabla \cdot \boldsymbol{U} = 0, \tag{1}$$

$$\frac{\partial \rho \boldsymbol{U}}{\partial t} + \nabla \cdot (\rho (\boldsymbol{U} - \boldsymbol{U}_g)\boldsymbol{U}) = -\nabla p_d - \boldsymbol{g} \cdot \boldsymbol{x} \nabla \rho + \nabla \cdot (\mu_{eff} \nabla \boldsymbol{U}) + (\nabla \boldsymbol{U}) \cdot \nabla \mu_{eff} + \boldsymbol{f}_\sigma + \boldsymbol{f}_s, \tag{2}$$

where $\boldsymbol{U}$ is the velocity field, $\boldsymbol{U}_g$ is the grid nodes velocity; $p_d = p - \rho \boldsymbol{g} \cdot \boldsymbol{x}$ is the dynamic pressure; $\mu_{eff} = \rho(\nu + \nu_t)$ is the effective dynamic viscosity, in which ν and ν_t are the kinematic viscosity and the eddy viscosity respectively; ν_t is obtained with the k-ω SST turbulence model[13]; $\boldsymbol{f}_\sigma$ is the surface tension term in the 2-phase model.

The solution of momentum and continuity equations is implemented with the pressure-implicit spit operator (PISO) algorithm[14]. The pressure solution on bulkhead is also based on the PISO algorithm. This method uses a predictor-corrector in solving the pressure-velocity coupling, and utilizes a collocated grid method[15].

1.2 6-DOF motions

To compute the ship motion in waves, a fully 6-DOF module with multiple bodies is implemented. The more details about the 6-DOF motion module can be found in Shen et al.[10]. 2 coordinate systems are used to solve the 6-DOF equation, as mentioned in fig. 1. The coordinate (X,Y,Z) presents the earth-fixed system and (X',Y',Z') presents the body-fixed system. The displacement of the ship in earth-fixed is described as $(\boldsymbol{x}_1,\boldsymbol{x}_2)=(x,y,z,\varphi,\theta,\psi)$, which denotes translation and rotation angles of the ship, representing motions of surge, sway, heave, roll, pitch and yaw, respectively. $(\boldsymbol{v}_1,\boldsymbol{v}_2)=(u,v,w,p,q,r)$ denotes the velocities of ship in earth-fixed coordinate system, which can be transformed to the body-fixed coordinate system by equations given below:

$$\boldsymbol{v}_1=\boldsymbol{J}_1^{-1}\cdot\dot{\boldsymbol{x}}_1,\ \boldsymbol{v}_2=\boldsymbol{J}_2^{-1}\cdot\dot{\boldsymbol{x}}_2, \tag{3}$$

where $\boldsymbol{J}_1$, $\boldsymbol{J}_2$ are the transformation matrices based on the Euler angle. The forces and moments are projected onto the earth-fixed system in the following way:

$$\boldsymbol{F}_s=(X_s,Y_s,Z_s)=\boldsymbol{J}_1^{-1}\cdot\boldsymbol{F}_e,\ \boldsymbol{M}_s=(K_s,P_s,N_s)=\boldsymbol{J}_1^{-1}\cdot\boldsymbol{M}_e, \tag{4}$$

where $\boldsymbol{M}_s$ and $\boldsymbol{F}_s$ are moment and force in ship coordinate respectively, $\boldsymbol{M}_e$ and $\boldsymbol{F}_e$ are moment and force of earth coordinate respectively.

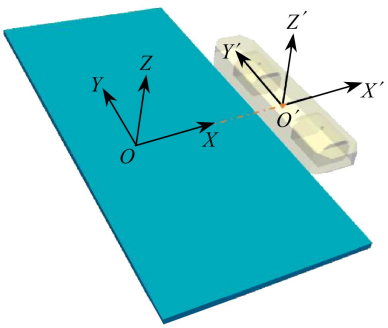

Fig. 1 The earth-fixed and the body-fixed coordinate systems

1.3 Dynamic deforming mesh

The ship motion and tank sloshing are solved as a whole, thus only the ship motion need the implementation of the moving-mesh technique. In this paper, a kind of dynamic deforming mesh is used. The mesh deforms during the computation according to ship motion. The positions of the mesh nodes in the field are solved with the Laplace's equation of variable diffusivity:

$$\nabla\cdot(\gamma\nabla\boldsymbol{x}_g)=0, \tag{5}$$

where $\boldsymbol{x}_g$ is the displacement of the mesh node; γ is the diffusivity field, determined by

$$\gamma=\frac{1}{r^2}, \tag{6}$$

where r is the distance between cell center and the moving boundary.

1.4 Volume of fluid method

To capture the free surface in the external region and the sloshing surface in the inner tanks, the VOF method with bounded compression techniques is applied to control numeri-

cal diffusion and capture the 2-phase interface efficiently. The VOF transport equation is described below:

$$\frac{\partial \alpha}{\partial t} + \nabla \cdot [(\boldsymbol{U} - \boldsymbol{U}_g)\alpha] = 0, \tag{7}$$

where α is the volume of fraction, indicating the relative proportion of fluid in each cell and its value is always between 0 and 1:

$$\begin{cases} \alpha = 0, & \text{air}, \\ \alpha = 1, & \text{water}, \\ 0 < \alpha < 1, & \text{interface}. \end{cases} \tag{8}$$

To capture the sharp interface and ensure conservation and boundedness, an extra term is added into the VOF transport equation:

$$\frac{\partial \alpha}{\partial t} + \nabla \cdot [(\boldsymbol{U} - \boldsymbol{U}_g)\alpha] + \nabla \cdot [\boldsymbol{U}_r(1 - \alpha)\alpha] = 0. \tag{9}$$

The added term is non-zero only at the interface, thus it doesn't affect the solution in other regions except the interface. $\boldsymbol{U}_r$ in eq.(9) is the velocity field used to compress the interface. It is normal to the interface so it does not affect the flow along the interface. The description of $\boldsymbol{U}_r$ is given below:

$$\boldsymbol{U}_r = \boldsymbol{n}_f \min\left\{ c_\alpha \frac{|\varphi|}{|\boldsymbol{S}_f|}, \max\left(\frac{|\varphi|}{|\boldsymbol{S}_f|} \right) \right\}, \tag{10}$$

where φ is the face volume flux, $\boldsymbol{S}_f$ is the normal vector of the cell face. The recommended value of c_α is 1, which maintains the sharp interface.

Besides, the surface tension term in eq.(2) is defined as

$$\boldsymbol{f}_\sigma = \sigma \kappa \nabla \alpha, \tag{11}$$

where σ is the surface tension coefficient, which set to 0.07 kg/s^2; κ is the curvature of the surface interface, determined by volume of fraction α:

$$\kappa = -\nabla \cdot (\nabla \alpha / |\nabla \alpha|). \tag{12}$$

1.5 Wave generation & damping

The incoming regular wave is generated by imposing the boundary conditions of α and $\boldsymbol{U}$ at the inlet. The linear Stokes wave in deep water is applied for the wave generation.

$$\xi(x,t) = a\cos(kx - \omega_e t), \tag{13}$$

$$u(x,y,z,t) = a\omega e^{kz}\cos(kx - \omega_e t), \tag{14}$$

$$w(x,y,z,t) = a\omega e^{kz}\sin(kx - \omega_e t), \tag{15}$$

where ξ is the wave elevation; a is the wave amplitude; k is the wave number; u, w are the ship velocity; ω is the natural frequency of wave; ω_e is the encounter frequency, in this condition, $\omega_e = \omega$.

2 Geometry and conditions

2.1 Geometry

To validate the present method, the LNG FPSO ship model with 2 prismatic tanks with 20% ~ 20% filling ratios is considered. The main parameters of the LNG FPSO ship are

shown in table 1. For comparison with experiments done by Nam et al.[5], this paper selects the LNG FPSO ship model with a scaling factor of 1/100, the full-scale length being 284 m. The width of the 2 tanks is the same but their lengths are different. Fig. 2 shows the details of the inner LNG tanks and their arrangement in the FPSO ship.

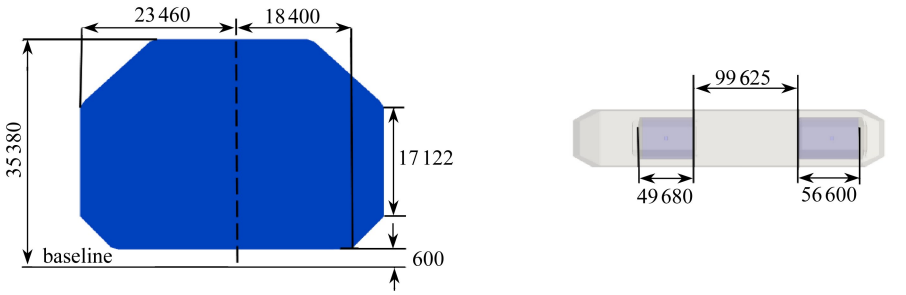

(a) The tank cross section(unit: mm) (b) The tank arrangement in the ship (unit: mm)

Fig. 2 The LNG tank model

Table 1 The main parameters of the LNG FPSO ship

parameter	full scale	model scale
scaling factor	1	1/100
length between perpendiculars L_{PP} /m	285	2.85
maximum beam of waterline B_{WL} /m	63	0.63
draft D_T /m	13	0.13
displacement Δ /m^3	220 017.6	220.017 6
natural period of roll $T_{\varnothing}$ /s	13	1.3
vertical center of gravity(from keel) K_G /m	16.5	0.165
radius of gyration K_{xx} /m	19.45	0.194 5
radius of gyration K_{yy} /m	71.25	0.712 5

2.2 Meshes

The selected domain is described as $-1.0L_{pp} < x < 2.0L_{pp}$, $-1.5L_{pp} < y < 1.5L_{pp}$, $-1.0L_{pp} < z < 1.0L_{pp}$. The meshes are generated with snappyHexMesh, an automesh generation utility provided by OpenFOAM. The total cell numbers are around 2.1×10^6, and the LNG tanks have 0.5×10^6 cells. The mesh details are shown in fig. 3. Fig.3(c) shows 2 small tunnels connected to the LNG tanks in the external regions, which can keep the pressure inside the tanks the same as that in the external regions and simplify the computations. Meanwhile, the attached tunnels make the computation fully coupled.

2.3 Computational conditions

To ignore the influence of water depth, Stokes first deep water is chosen. To be compared with the existing experimental results, the wave height is set to 0.025 m. 4 different incident wave frequencies are considered, and listed in table 2. The settings for numerical computations are illustrated in fig. 4, the wave direction angle is 90°. To ensure the mass

conservation in wave generation, a wave sponge layer is set in the computational domain.

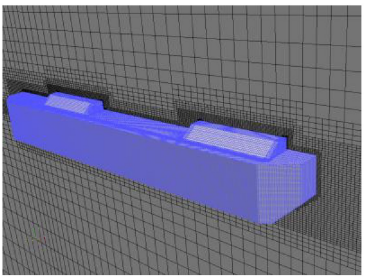

(a) The bow

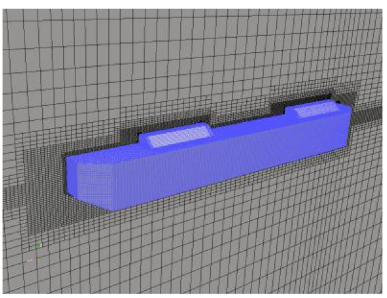

(b) The stern

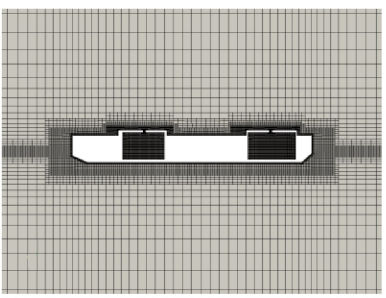

(c) The ship hull with tanks

Fig. 3 Demonstrations of meshes

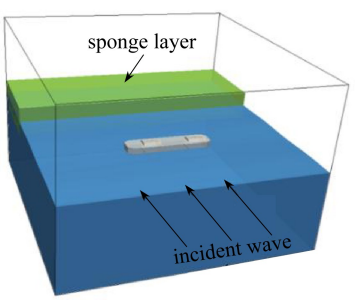

Fig. 4 Setup of the computational domain

3 Validation

The ship motion are restricted to 3-DOFs, heave, pitch and roll. The normalized motion amplitude and natural frequency are considered for comparison with experimental data. The normalized roll motion is given as $R_n = \theta B/(2A)$ [8], in which θ is the maximum degree of roll motion, B is the ship beam and A is the wave amplitude. The normalized heave motion is given as ξ/A, in which ξ is the maximum value of heave motion; and the normalized natural frequency is given as $T_n = \omega(L/g)^{1/2}$, in which ω is the natural frequency of water, L represents the ship length. Table 2 shows 4 different simulation setups with a low-filling ratio. In comparison with the existing experimental data, the simulations are all under the same incident wave height. 4 different incident wave frequencies are considered. Fig. 5

indicates the comparison of results between the present work and the experiment. The present results show well agreement with the experimental data, which proves that our methods are reliable.

Table 2 Incident wave conditions in present investigation

case	incident wave frequency T_n	incident wave height h /m	filling ratio
1	1.5	0.025	20% ~ 20%
2	2.5		
3	2.65		
4	3		

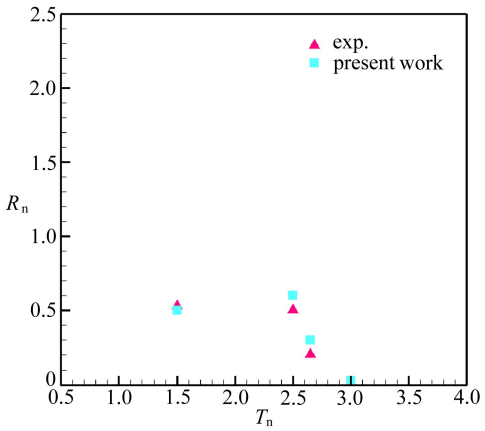

Fig. 5 Comparison between the present numerical results and the experimental data

4 Results

The comparison of ship motion between non-filling condition (0% ~ 0%) and low-filling condition (20% ~ 20%) is given below. Fig. 6 shows the time histories of roll and heave motions in these 2 filling conditions under the same incident wave frequency and amplitude. The incident wave frequency T_n is set to 2.5, and the incident wave height is 0.025 m. The coupling effects of ship motion and tank sloshing are not obvious in heave motion, shown in fig. 6(a), but quite significant in roll motion, shown in fig. 6(b). The partially filled tanks reduce the roll amplitudes of ship motion. For further study on the coupling effects in this of low-filling condition, a large wave amplitude and 3 different incident wave frequencies are considered.

4.1 Ship motion

To observe the large motion and violent flow in inner tanks, the wave height is set to 0.1 m. 3 incident wave frequencies are selected at $\omega(L/g)^{1/2} = 2.25$, $\omega(L/g)^{1/2} = 2.5$ and $\omega(L/g)^{1/2} = 3$. Fig. 7 shows the time histories of heave and roll motions under 3 different incident wave conditions. The amplitudes of heave motion are almost the same, while the amplitudes of roll motion show much difference. The amplitudes of roll motion in condition

$\omega(L/g)^{1/2}$ = 3 is much smaller than in the other 2 conditions.

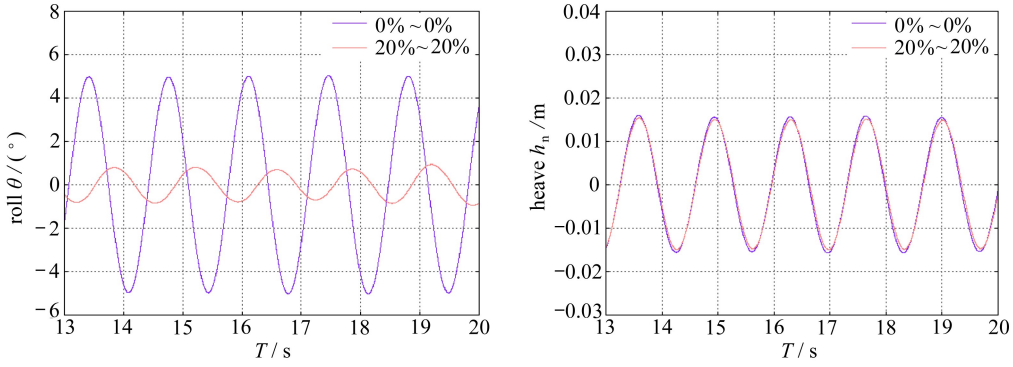

(a) The roll motion (b) The heave motion

Fig. 6 Time histories of heave and roll motions with different filling ratios

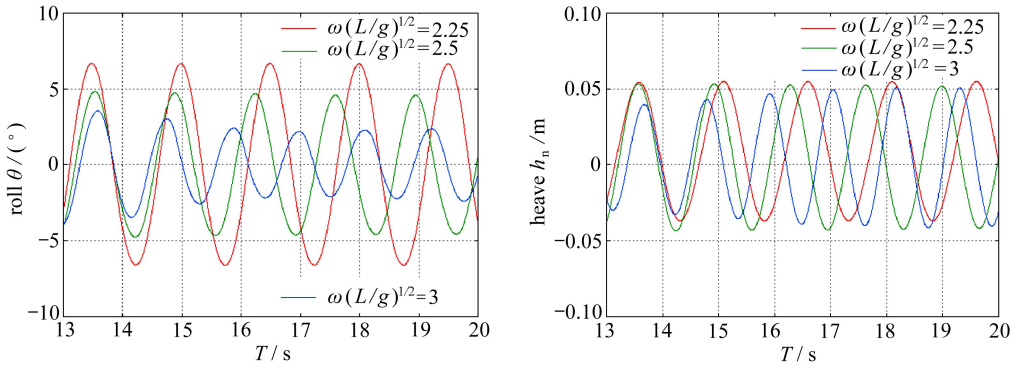

(a) The roll motion (b) The heave motion

Fig. 7 Time histories of ship roll motion and heave motion under different incident wave frequencies

Table 3 shows at the same incident wave frequency, the influence of incident wave amplitude on the coupling effects. It can be seen from fig. 7(a) that the time history of roll motion at $\omega(L/g)^{1/2}$ = 2.5 is much larger than that in fig. 6(a), where the wave amplitude is smaller. However, table 3 indicates that the normalized roll motions of these 2 cases are almost the same. While at $\omega(L/g)^{1/2}$ = 3 the normalized roll motion in larger wave is larger than that in smaller wave. That is, the incident wave amplitude not only affects the ship motion, but also influences the internal tank sloshing. The nonlinearity of the sloshing in tanks makes the normalized roll motion of the ship change in a non-monotonic way.

Table 3 Comparison of normalized roll motion between 2 different wave amplitudes

case	incident wave frequency T_n	incident wave height h/m	normalized roll motion R_n
1	2.5	0.025	0.500
		0.1	0.506
2	3	0.025	0.010
		0.01	0.264

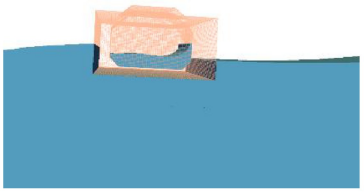

(a) $\omega(L/g)^{1/2} = 2.25$

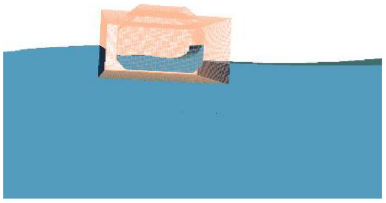

(b) $\omega(L/g)^{1/2} = 2.5$

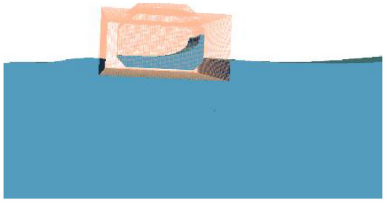

(c) $\omega(L/g)^{1/2} = 3$

Fig. 8 Ship motions coupled with tank sloshing under waves

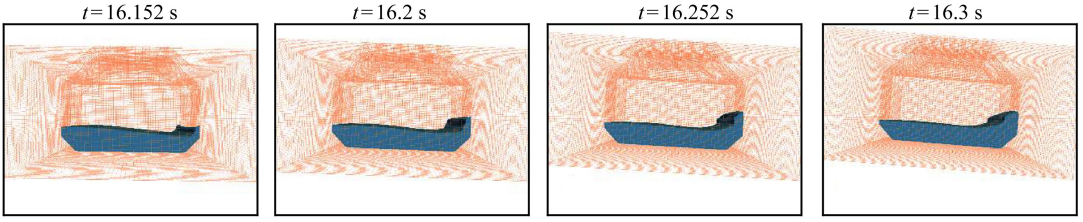

(a) $\omega(L/g)^{1/2} = 2.25$

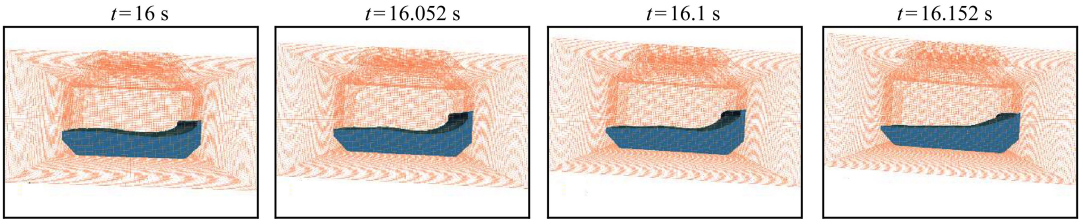

(b) $\omega(L/g)^{1/2} = 2.5$

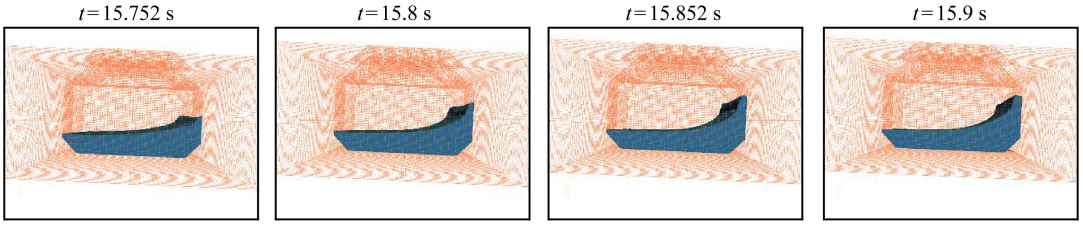

(c) $\omega(L/g)^{1/2} = 3$

Fig. 9 Snapshots of LNG FPSO tank sloshing at different incident wave frequencies

Fig. 8 gives the snapshots of ship motion and tank sloshing under 3 different wave conditions. The snapshots show the same inner tank state when free surface in tanks reaches the bulkhead and the flow peak splashes to the highest point. However, the state of ship is

different. The time of these 3 snapshots from left to right are 16.052 s, 16.251 s and 16.010 s. It can be seen from fig. 7(a) that at these time points, the ship motions under the conditions of both $\omega(L/g)^{1/2} = 2.25$ and $\omega(L/g)^{1/2} = 2.5$ are going to the peak, while the ship motion under $\omega(L/g)^{1/2} = 3$ has passed the peak already. That is, when the flow in inner tanks reaches the bulkhead, it will impose rotation moments on the ship. In the conditions of $\omega(L/g)^{1/2} = 2.25$ and $\omega(L/g)^{1/2} = 2.5$, the rotation moment is imposed on the ship when the ship is going to the right side. Whereas in the condition of $\omega(L/g)^{1/2} = 3$, the ship is going to left side, and the moments of inner tanks imposed on the ship will reduce the roll motion. Therefore, the phase difference between ship motion and tank sloshing affects the ship motion.

4.2 Tank sloshing

The phenomenon of inner tank sloshing makes another way to analyze the coupling effects. Fig. 9 shows the local view of LNG tank sloshing at these 3 different incident wave frequencies. The 4 snapshots of the inner tank show the process from the generation of the peak of free surface in the tank to its highest point. Fig. 9(a) shows the overturning process of the tank sloshing. The crest of the fluid reaches the bulkhead and then a climb happens. The climb phenomena are all observed at 3 different incident wave frequencies, whereas at $\omega(L/g)^{1/2} = 3$, the sloshing is more violent. The flow in tank climbs almost near the upper corner of the tank.

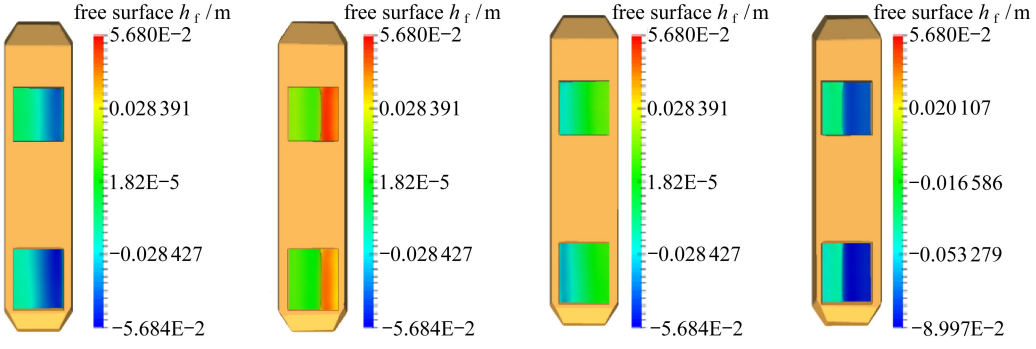

(a) $t = T_0$ (b) $t = T_0 + T/4$ (c) $t = T_0 + 2T/4$ (d) $t = T_0 + 3T/4$

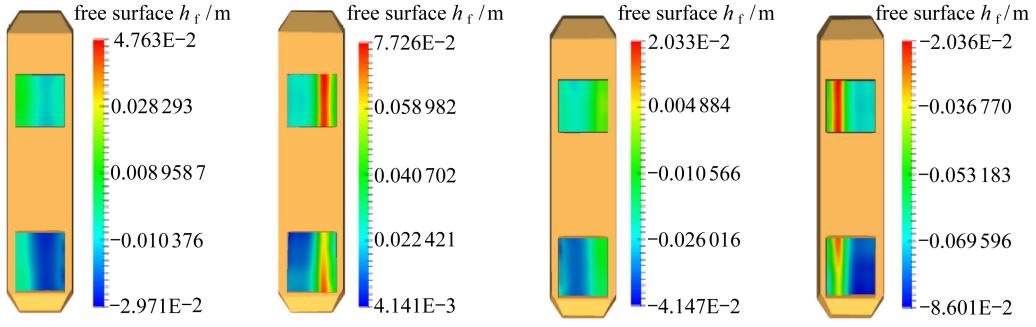

(e) $t = T_0$ (f) $t = T_0 + T/4$ (g) $t = T_0 + 2T/4$ (h) $t = T_0 + 3T/4$

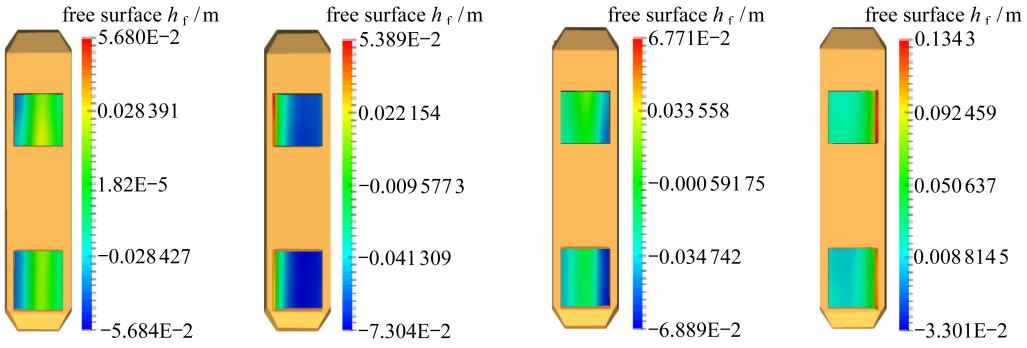

(i) $t = T_0$ (j) $t = T_0 + T/4$ (k) $t = T_0 + 2T/4$ (l) $t = T_0 + 3T/4$

Fig. 10 Contours of amplitudes of sloshing flow in inner tanks at different incident wave frequencies

((a)~(d): $\omega(L/g)^{1/2} = 2.25$; (e)~(h): $\omega(L/g)^{1/2} = 2.5$; (i)~(l): $\omega(L/g)^{1/2} = 3$)

To observe the flow in tanks in detail, the contour of inner fluid is investigated. Fig. 10 shows the contours of inner fluid, colored with the amplitude of surface in tanks. A group of 4 snapshots are within one ship motion period. At $\omega(L/g)^{1/2} = 2.25$, we can see an overturning phenomenon in tanks. The flow surface that reaches the bulkhead turns over to become a new free surface. At $\omega(L/g)^{1/2} = 2.5$, although the overturning phenomenon is still observed in fig. 9(b), the crest of fluid in the tank does not cover the free surface. The crest of fluid in the tank propagates from one side of the tank to the other side. At $\omega(L/g)^{1/2} = 3$, the crest of fluid is observed only near the bulkhead. That is, the crest of fluid reaches the bulkhead and then the overturning phenomenon happens, the energy in the tank drives the fluid up to the upper corner of the tank, but the energy is not large enough to make the crest to spread further. As for the amplitude of the sloshing fluid, the fluid crest at $\omega(L/g)^{1/2} = 3$ is the largest, which shows the fluid in the tank climbs the highest among the 3 cases.

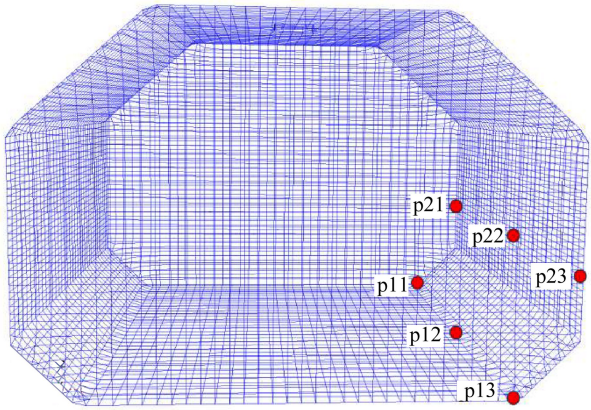

Fig. 11 The setup of pressure probes

Since the flow in the inner tank is violent, the impact pressure on the bulkhead needs investigation. Fig. 11 shows the pressure probes on the bulkhead. The 1st set of pressure probes, p11, p12, p13 are put on the slope corner near the tank bottom, and the 2nd set,

p21, p22, p23 are placed at the same level as the outside free surface. When the ship keeps still, the second set of pressure probes give the readings of 0.

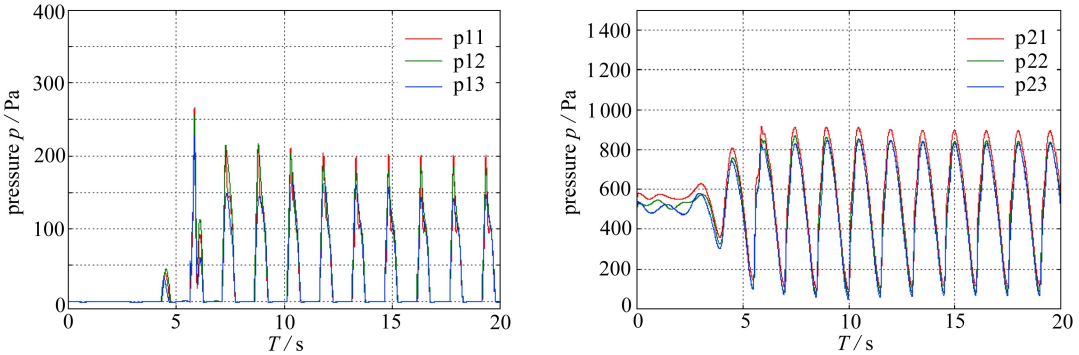

(a) $\omega(L/g)^{1/2} = 2.25$

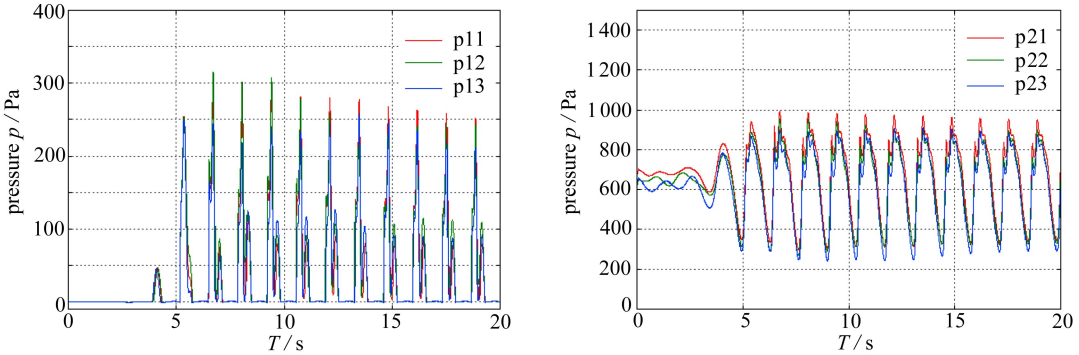

(b) $\omega(L/g)^{1/2} = 2.5$

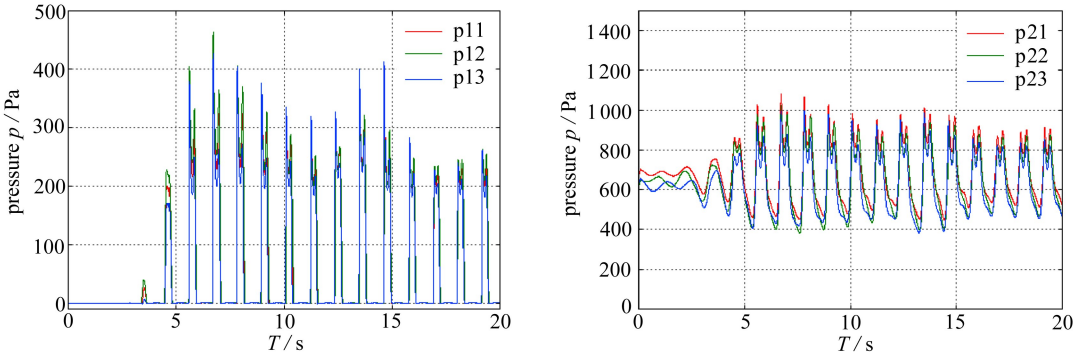

(c) $\omega(L/g)^{1/2} = 3$

Fig. 12 Pressure results from various probes at different wave frequencies

Fig. 12 shows the pressure results on various probes at different incident wave frequencies. At all incident wave frequencies, the impulsive pressures on the bulkhead are observed. The fluid in low-filling tanks flows violently, thus generates impulsive pressures on the bulkhead. For $\omega(L/g)^{1/2} = 3$, the impulsive pressure peaks at p11, p12 and p13 are the largest due to the fluid climbing highest on the bulkhead. The ranges of pressure values at p21, p22 and p23 do not show much difference. Combining the climb phenomenon in fig. 9

with that in fig. 10, we can see that the fluid crest at $\omega(L/g)^{1/2} = 2.25$ is the smallest, thus the largest peaks at p21, p22 and p23 is still the smallest.

5 Conclusions

In this paper, the ship motion fully coupled with the internal tank sloshing in beam waves is investigated. To study the violent flow in tanks of low-filling condition, the 20% ~ 20% filling ratio is chosen. The numerical simulations are performed with the CFD method by our in-house solver naoe-FOAM-SJTU. The internal tank sloshing and external wave excitation are computed simultaneously by solving RANS equations. The pressure and velocity are solved with the PISO algorithm. The free surface is captured with the VOF method. 4 different incident wave frequencies are considered under the low-filling condition and the results show good agreement with those from the existing experiments. The conclusions are drawn below:

The coupling effects are investigated and observed. With a wavelength equal to 1.005 times the ship length, the sloshing has remarkable effect on the roll motion in the beam wave condition. The low-filling ratio tanks reduce the ship motion under this incident wave condition. In the simulation of different incident wave frequencies, when the normalized frequency equals to 3, the normalized roll motion in the low-filling condition decreases rapidly.

The influence of wave amplitude is non-monotonic. The value of normalized roll motion in large wave is almost the same as that in small wave at $\omega(L/g)^{1/2} = 2.5$, but is larger than that in small wave at $\omega(L/g)^{1/2} = 3$.

Different incident wave frequencies give different excitations on tank sloshing, and the tank sloshing affect ship motion in return. The overturning phenomenon is observed at all 3 different incident wave frequencies. The intensity of the sloshing is various due to the excitations. In the present study, when the crest of fluid in the tank climbs low, a new surface will turn over and cover the original free surface; when the crest climbs higher, it will spread to the other side of the tank; when the peak of fluid climbs and nearly reaches the upper corner, the crest of fluid will turn over on the bulkhead. The impact pressure on bulkhead is also investigated. Pressure probes are set on the bottom of the tank and at the same level with the outer still water. Impulsive pressures are observed, and the time histories of the pressure values correspond with the phenomena of tank sloshing.

Acknowledgments

This work is supported by the National Natural Science Foundation of China (51379125; 51490675; 11432009; 51579145; 11272120); the Chang Jiang Scholars Program of China(T2014099); the Program for Professor of Special Appointment (Eastern Scholar) at Shanghai Institutions of Higher Learning (2013022) and the Innovative Special Project of Numerical Tank of Ministry of Industry and Information Technology of China (2016-23/

09), to which the authors are most grateful.

References:

[1] Mikelis N E, Miller J K, Taylor K V. Sloshing in partially filled liquid tanks and its effect on ship motions: numerical simulations and experimental verification[J]. *Royal Institution of Naval Architects Transactions*, 1984, **126**: 267-281.

[2] Malenica S, Zalar M, Chen X B. Dynamic coupling of seakeeping and sloshing[C]//*Thirteenth (2003) International Offshore and Polar Engineering Conference*. Honolulu, Hawaii, 2003: 25-30.

[3] Kim Y A. A numerical study on sloshing flows coupled with ship motion—the anti-rolling tank problem[J]. *Journal of Ship Research*, 2002, **46**(1): 52-62.

[4] Kim Y, Shin Y S, Lin W M, Yue D K P. Study on sloshing problem coupled with ship motion in waves[C]//*The Eighth International Conference on Numerical Ship Hydrodynamics*. 2003.

[5] Nam B W, Kim Y, Kim D W, Kim Y S. Experimental and numerical studies on ship motion responses coupled with sloshing in waves[J]. *Journal of Ship Research*, 2009, **53**(2): 68-82.

[6] Serván-Camas B, Cercós-Pita J L, Colom-Cobb J, García-Espinosa J, Souto-Iglesias A. Time domain simulation of coupled sloshing-seakeeping problems by SPH-FEM coupling[J]. *Ocean Engineering*, 2016, **123**: 383-396.

[7] LI Yu-long, ZHU Ren-chuan, MIAO Guo-ping, FAN Ju. Simulation of tank sloshing based on OpenFOAM and coupling with ship motions in time domain[J]. *Journal of Hydrodynamics, Ser B*, 2012, **24**(3): 450-457.

[8] JIANG Sheng-chao, TENG Bin, BAI Wei, GOU Ying. Numerical simulation of coupling effect between ship motion and liquid sloshing under wave action[J]. *Ocean Engineering*, 2015, **108**: 140-154.

[9] Sen D. Time-domain computation of large amplitude 3D ship motions with forward speed[J]. *Ocean Engineering*, 2002, **29**(8): 973-1002.

[10] SHEN Zhi-rong, YE Hai-xuan, WAN De-cheng. Motion response and added resistance of ship in head waves based on RANS simulations[J]. *Chinese Journal of Hydrodynamics*, 2012, **27**(6): 621-633.

[11] WANG Jian-hua, WAN De-cheng, CHEN Gang. Comparative studies of 3-D LNG tank sloshing based on the VOF and IMPS methods[C]//*The 26th International Ocean and Polar Engineering Conference*. Rhodes, Greece, 2016.

[12] Shen Z R, Wan D C. Numerical simulations of large-amplitude motions of KVLCC2 with tank liquid sloshing in waves[C]//*2nd International Conference on Violent Flows*. 2012: 129-156.

[13] Dhakal T P, Walters D K. Curvature and rotation sensitive variants of the *k*-Omega SST turbulence model[C]//*ASME 2009 Fluids Engineering Division Summer Meeting*. Vail, Colorado, 2009: 2221-2229.

[14] Issa R I. Solution of the implicitly discretised fluid flow equations by operator-splitting[J]. *Journal of Computational Physics*, 1986: **62**(1): 40-65.

[15] Rhie C M, Chow W L. Numerical study of the turbulent flow past an airfoil with trailing edge separation[J]. *AIAA Journal*, 1983, **21**(11): 1525-1532.

FPSO 船与低充水率下 LNG 液舱晃荡耦合运动的数值模拟

庄 园, 万德成

(海洋工程国家重点实验室(上海交通大学);
上海交通大学 船舶海洋与建筑工程学院; 高新船舶与深海开发装备协同创新中心, 上海 200240)

摘要: 应用数值模拟方法对 FPSO 船舶运动与 LNG 液舱晃荡耦合问题进行了研究.这种全耦合问题的研究基于开源平台 OpenFOAM 开发的船舶与海洋工程水动力 CFD 求解器——naoe-FOAM-SJ-TU 进行计算.液舱内部流场与外部流场同时求解.采用带有两个 LNG 液舱的 FPSO 船作为对象进行数值模拟,船舶放开 3 个自由度运动,并在 90°浪向的规则波中进行模拟.液舱充水率为 20% ~ 20%,低于船外自由水面高度.这种低充水率的液舱会大大减少船舶的横摇运动,并且舱内的流体情况较为复杂.考虑了 4 种不同的入射波频率下船舶的运动,与实验结果进行了对比.数值模拟结果与实验结果对比吻合良好,验证了数值求解方法的可靠性.还对大波高情况下带有低充水率 LNG 液舱的船舶运动进行了数值模拟分析.在船舶运动与液舱晃荡全耦合情况下,观察到了液舱内流体的剧烈晃荡和舱壁的脉冲压力.

关 键 词: LNG 液舱晃荡; 耦合运动; 低充水率; naoe-FOAM-STJU 求解器

基金项目: 国家自然科学基金(51379125; 51490675; 11432009; 51579145; 11272120);长江学者奖励计划(T2014099)

引用本文/Cite this paper:

ZHUANG Yuan, WAN De-cheng. Numerical study on coupling effects of FPSO ship motion and LNG tank sloshing in low-filling conditions[J]. *Applied Mathematics and Mechanics*, 2016, **37**(12): 1378-1393.

庄园, 万德成. FPSO 船与低充水率下 LNG 液舱晃荡耦合运动的数值模拟[J]. 应用数学和力学, 2016, **37**(12): 1378-1393.